NUMERICAL SIMULATION OF THE MOTION OF A MICROPOLAR CASSON FLUID THROUGH A POROUS MEDIUM OVER A STRETCHING SURFACE

by

Nabil T. M. El-DABE[a], Galal M. MOATIMID[a], Abd-Elhafez A. ELSHEKHIPY[b], and Naglaa F. ABALLAH[a*]

[a] Department of Mathematics, Faculty of Education, Ain Shams University, Roxy, Heliopolis, Cairo, Egypt
[b] Mathematics Department, Faculty of Science, Imam Abdulrahman Bin Faisal University, Al-Dammam, Kingdom of Saudi Arabia

Original scientific paper
https://doi.org/10.2298/TSCI180604008E

The present study examines the motion of a micropolar non-Newtonian Casson fluid through a porous medium over a stretching surface. The system is pervaded by an external uniform magnetic field. The heat transfer and heat generation are taken into consideration. The problem is modulated mathematically by a system of non-linear PDE which describe the equations of continuity, momentum, and energy. Suitable similarity solutions are utilized to transform the system of equation ordinary non-linear differential equations. In accordance with the appropriate boundary conditions, are numerically solved by means of the finite difference technique. Also, the system is solved by using multistep differential transform method. The effects of the various physical parameters, of the problem at hand, are illustrated through a set of diagrams.

Key words: *micropolar Casson fluid, porous medium, finite difference method, multi-step differential transform method*

Introduction

The theory of micropolar fluid has been a field of very active research because it takes into consideration the microscopic influences arising from the local structure and micro-motions of the fluid elements. The theory is expected to provide a mathematical model, which can be utilized to describe the behavior of non-Newtonian fluids such as liquid crystals, polymeric fluids, paints, animal blood, Ferro liquids, colloidal fluids, *etc*. The concept of simple micro-fluids to characterize concentrated suspensions of neutrally buoyant deformable particles in a viscous fluid where the individuality of substructures affects the physical outcome of the flow was discussed by Eringen [1]. Such fluids models can be used to rheological describe normal human blood, polymeric suspensions, *etc*. Also, they have found applications in physiological and engineering problems. Ali and Hayat [2] carried out a study of peristaltic motion of an incompressible micropolar fluid in an asymmetric channel, the flow analysis has been developed for low Reynolds number and long wavelength case. Also, they compared the results for micropolar fluid with those for Newtonian fluid. The influences of thermal radiation on MHD axisymmetric stagnation point flow and heat transfer of a micropo-

* Corresponding author, e-mail: dr_nagla_1@yahoo.com

lar fluid over a shrinking sheet was discussed by Shahzad, *et al*. [3]. In another paper, Eldabe, *et al*. [4] studied MHD peristaltic flow with heat and mass transfer of micropolar biviscosity fluid through a porous medium between two co-Axial tubes. They obtained the effects of physical parameters on Nusselt number and Sherwood number. Nazeer *et al*. [5] discussed the numerical simulation of MHD flow of micropolar fluid inside a porous inclined cavity with uniform and non-uniform heated bottom wall. Free convective micropolar fluid-flow and heat transfer over a shrinking sheet with heat source was delineated by Mishra *et al*. [6]. For more details and thermos physical properties of micropolar fluid see ref [7-12].

Flow through a porous medium has several practical applications especially in geophysical fluid dynamics. Examples of natural porous media are sandstone, beach sand, the human lung, limestone, bile duct and gall bladder with stones in small blood vessels. Eldabe, *et al*. [13] constructed heat and mass transfer of MHD pulsatile flow of Casson fluid with couple stress through porous medium. Mekheimer [14] delineated the non-linear peristaltic transport through a porous medium in an inclined planar channel. Zueco and Ahmed [15] discussed the combined heat and mass transfer by mixed convection MHD flow along a porous plate with chemical reaction in presence of heat source, and they found that the flow velocity, the fluid temperature, and the induced magnetic field decrease with the increase in the destructive chemical reaction. In another paper, El-Dabe *et al*. [16], scrutinized the influence of partial slip on peristaltic flow of a Sisko fluid with mild stenosis through a porous medium and found that the Darcy's coefficient of the fluid restrains the velocity.

The Casson fluid model is used to predict blood flow in arteries at very low shear rate. Also, it utilized in perception flow behavior of pigment oil suspensions of the printing ink type. The shear stress-shear rate relation given by Casson satisfactorily describes the properties of many polymers over a wide range of shear rates [17]. A numerical investigation of micropolar Casson fluid over a stretching sheet with internal heating was reported by Mehmoo *et al*. [18]. Impact of inclined magnetic field on micropolar Casson fluid. Further, the influence of inclined magnetic field on micropolar Casson fluid using Keller box algorithm was studied by Iqbal *et al*. [19].

The study of stagnation point flow was pioneered by Hiemenz [20]. A flow can be stagnated by a solid wall, a free stagnation point or a line can exist in the interior of the fluid domain Shateyi and Makinde [21]. Bhattacharyya *et al*. [22] scrutinized the effects of partial slip on steady boundary-layer stagnation-point flow of an incompressible fluid and heat transfer towards a shrinking sheet. The relevance of this study attracted Motsa *et al.* [23] to formulate mathematical equation governing Maxwell fluid for 2-D stagnation flow towards a shrinking sheet and analyzed the flow behavior extensively using similarity variables together with successive linearization method. Javed and Ghaffari [24] addressed the numerical study of non-Newtonian Maxwell fluid in the region of oblique stagnation point flow over a stretching sheet. Mustafa *et al.* [25] scrutinized the heat transfer in MHD stagnation point flow of a ferrofluid over a stretchable rotating disk. Further, the heat transfer analysis of unsteady oblique stagnation point flow of elastico-viscous fluid due to sinusoidal wall temperature over an oscillating-stretching surface: A numerical approach was deliberated by Ghaffari *et al*. [26].

Internal energy generation can be explained as a scientific method of generating heat energy within a body by a chemical, electrical or nuclear process. Natural-convection induced by internal heat generation is a common phenomenon in nature. Example includes motion in the atmosphere where heat is generated by absorption of sunlight [27]. Crepeau and Clarksean [28] carried out a similarity solution for a fluid with an exponential decaying heat generation term and a constant temperature vertical plate under the assumption that the fluid under consideration has an internal volumetric heat generation. In many situations, there may be appre-

ciable temperature difference between the surface and the ambient fluid. This necessitates the consideration of temperature dependent heat sources that may exert a strong influence on the heat transfer characteristics, (see Salem *et al*. [29]. In another paper, El-Aziz and Salem [30] has stated that exact modelling of internal heat generation/absorption is quite difficult and argued that some simple mathematical models can express its average behavior for most physical situations. Muhammad *et al*. [31] debated the rotating flow of magneto hydrodynamic carbon nanotubes over a stretching sheet with the impact of non-linear thermal radiation and heat generation/absorption. For more details and application in this direction see [32-37].

The micropolar casson fluid problems with heat generation and porous medium are modeled by a set of coupled non-linear PDE, combined with the geometrical complexity of these problems which makes analytical or closed form solutions virtually impossible to obtain. Therefore, a substantial amount of research work has been invested in order to obtain satisfactory solutions. The present investigation uses the finite difference methods (FDM) as well as the multi-step differential transformed method (Ms-DTM) methods to overcome the highly non-linear terms that appear in micropolar Casson fluid models. The Ms-DTM method accelerates the convergence of the series solution over large region and yields a series solution, this series will be truncated due to the required accuracy of solutions. This modified technique is verified through illustrative examples of non-chaotic or chaotic systems by Odibat, *et al*. [38]. Further, to get more accurate results Zait *et al*. [39], studied the statistical measures approximations for the Gaussian part of the stochastic non-linear damped Duffing oscillator solution process under the application of Wiener Hermite expansion linked by the Ms-DTM. The FDM is proposed by Courant *et al*. [40] in 1928. The FDM are numerical methods that give a solution the differential equations by approximating them with difference equations [41]. In another paper, Thomee [42] introduced a short history of numerical analysis of PDE to finite differences and finite elements.

The aim of the present work is to extend the work of Motsa *et al*. [23], to include the motion of micropolar Casson fluid in a porous medium. A detailed comparison between Ms-DTM and FDM methods is made to show an agreement between them. Moreover concluding remarks are summarized in the last section.

Mathematical formulations

It is convenient to use the Cartesian co-ordinates in 2-D, say x, y. The temperature at the stretched plane $y = 0$ is taken as T_w. Meanwhile, the temperature at ∞ is referred by T_∞, see fig. 1. A uniform magnetic field B_0 is acted upon the negative direction of the x-axis.

The constituting equations of continuity, conservation momentum, angular momentum, and energy with compressibility conditions are summarized [15, 20, 29]:

– continuity equation

$$\frac{\partial u}{\partial x}+\frac{\partial u}{\partial y}=0 \tag{1}$$

– the conservation momentum yields

$$u\frac{\partial u}{\partial x}+v\frac{\partial u}{\partial y}=U\frac{\partial U}{\partial x}+v\left(1+\frac{k}{\mu}+\frac{1}{\beta}\right)\frac{\partial^2 u}{\partial y^2}+\frac{k}{\rho}\frac{\partial N}{\partial y}+\left(\frac{\sigma {B_0}^2}{\rho}+\frac{\mu}{\rho K_d}\right)(U-u) \tag{2}$$

– the angular momentum equation

$$\rho\left(u\frac{\partial N}{\partial x}+v\frac{\partial N}{\partial y}\right)=\mu\left(1+\frac{k}{2}\right)\frac{\partial^2 N}{\partial y^2}-\mu k\left(2N+\frac{\partial u}{\partial y}\right) \tag{3}$$

– finally, the energy equation given

$$u\frac{\partial T}{\partial x}+v\frac{\partial N}{\partial y}=\alpha\frac{\partial^2 T}{\partial x^2}\left(U-u\right)^2+\frac{v}{c_p}\left(1+\frac{1}{\beta}\right)\left(\frac{\partial u}{\partial y}\right)^2+\frac{Q}{\rho c_p}\left(T-T_\infty\right) \tag{4}$$

It is convenient to consider the appropriate boundary condition [3]:

$$u=ax,\ v=0,\ N=-n\frac{\partial u}{\partial y},\ T=T_w,\ \text{at}\ \ y=0 \tag{5}$$

$$u\left(x\right)=bx,\ \ N\to 0,\ T\to T_\infty,\ \text{as}\ y\to\infty \tag{6}$$

where μ is the dynamics viscosity, k – the thermal diffusivity, ρ – the fluid density, N – the microrotation vector (or angular velocity), μ – the spin gradient viscosity, γ – the electric conductivity, K – the dimensionless velocity ratio parameter, B_0 – the strength of magnetic field, n – the b89 the Darcy permeability.

To simplify the analysis of solutions for the previous equations. It is convenient to consider the following procedure:

– the similarity is useful to convert the partial differential equation ODE,
– the dimensionless quantities are very important to provide the characteristic dimensionless number with its useful:

$$\eta=\left(\frac{a}{v}\right)^{1/2}y,\ u=axf'^{(\eta)},\ \ v=-\left(av\right)^{1/2}f'^{(\eta)},N=ax\left(\frac{a}{v}\right)^{1/2}g\left(\eta\right) \tag{7}$$

and

$$T=\Delta T\Theta\left(\eta\right)+T_\infty\ \ \text{or}\ \ \theta=\frac{T-T_\infty}{T_w-T_\infty} \tag{8}$$

Thus, eqs. (2)-(4) becomes:

– momentum yields

$$\left(1+\frac{k}{\mu}+\frac{1}{\beta}\right)f'''+ff''-f'^2+Kg'+\left(\mathrm{Ha}^2+S^2\right)\left(C-f'^2\right)=0 \tag{9}$$

– the angular momentum equation

$$\left(1+\text{—}\right)g''+fg'-f'g-K\left(2g\quad f''\right)=0 \tag{10}$$

– finally, the energy equation given

$$\frac{1}{\mathrm{Pr}}\theta''+f\theta'+\mathrm{Ec}\left(1+\frac{1}{\beta}\right)f''^2+\mathrm{Ha}^2\mathrm{Ec}\left(C-f'^2+B\theta\right)=0 \tag{11}$$

The corresponding boundary conditions become:

$$f\left(0\right)=0,\ \ f'\left(0\right)=1,\ \ f'\left(\infty\right)=C \tag{12}$$

$$\theta\left(0\right)=1,\ \theta\left(\infty\right)=0,\ \ g\left(0\right)-nf''\left(0\right),\ \ g\left(\infty\right)=0 \tag{13}$$

where $\mathrm{Ha}^2=\sigma_e B_0^2/\rho a$ is the Hartmann number, $S=1/(\mathrm{Da})^{1/2}$ is the porous medium shape factor parameter, $\mathrm{Pr}=\mu c_p/k_0$ – the Prandtl number, $\mathrm{Ec}=U^2/\Delta T c_p$ – the Eckert number, and $B=Q/a\rho c_p$ is the dimensionless heat generation/absorption parameter.

Multi-step differential equation method

Using similar arguments as given by [38]. The equations of motion as mentioned in (9)-(11) with the appropriate boundary conditions eqs. (12) and (13) are transformed:

– conversation of momentum yields

$$\left(1+\frac{k}{\mu}+\frac{1}{\beta}\right)(k+1)(k+2)(k+3)F(k+3)+K(k+1)G(k+1)-$$
$$-\left(\mathrm{Ha}^2+S^2\right)(k+1)F(k+1)+\left[\left(\mathrm{Ha}^2+S^2\right)c+c^2\right]\delta[k]+$$
$$+\sum_{r=0}^{k}(r+1)(r+2)F(r+2)F(k-r)-\sum_{r=0}^{k}(r+1)(r+2)F(r+1)F(k-r+1) \tag{14}$$

– the angular momentum equation gives

$$(1+K)(k+1)(k+2)G(k+1)-K\left\{2G[k]+(k+1)(k+2)F(k+2)\right\}+$$
$$+\sum_{r=0}^{k}(r+1)\left[G(r+1)F(k-r)-F(r+1)G(k-r)\right]=0 \tag{15}$$

– finally, the energy equation is given

$$\frac{1}{\mathrm{Pr}}(k+1)(k+2)\theta(k+2)+B\theta[k]-2\mathrm{Ha}^2\mathrm{Ec}C(k+1)F(k+1)+\mathrm{Pr}\,\mathrm{Ha}^2\mathrm{Ec}C^2\delta[k]+$$
$$+\sum_{r=0}^{k}(r+1)\theta(r+1)F(k-r)+\left(1+\frac{1}{\beta}\right)\cdot$$
$$\cdot\sum_{r=0}^{k}(r+1)(r+2)F(r+2)(k-r+1)(k-r+2)F(k-r+2)+$$
$$+\mathrm{Ha}^2\mathrm{Ec}\sum_{r=0}^{k}(r+1)F(r+1)(k-r+1)F(k-r+1)=0 \tag{16}$$

where $F[k]$, $G[k]$, and $\theta[k]$ are the differential transformation functions of $f[\eta]$, $g[\eta]$, and $\theta[\eta]$, respectively. The differential transform of the related boundary conditions are given by, respectively. The differential transform of the associated boundary conditions are given:

$$F[0]=0,\ F[1]=1,\ G[0]=-2nF[2],\ \theta[0]=1,$$
$$\sum_{r=0}^{k}F_k\left[\eta_\infty\right]^k=C,\ \sum_{r=0}^{k}G_k\left[\eta_\infty\right]^k=0,\ \sum_{r=0}^{k}\theta_k\left[\eta_\infty\right]^k=0 \tag{17}$$

By substituting from eq. (17) in eqs. (14)-(16), we obtain series of solutions to the velocity, microrotation and temperature distributions. They are achieved with the aid of MATHEMATICA 10 software.

Finite difference method

The implicit FDM is used to solve eqs. (9)-(11), see [42], subject to the boundary conditions of eqs. (12) and (13). This scheme is unconditionally stable and gives a better accuracy. We use a FDM to solve a system of differential eqs. (9)-(11). We reduce the order of these equations with the help of the substitution $q = f'$:

$$\left(1+\frac{k}{\mu}+\frac{1}{\beta}\right)q''+fq'-q^2+Kg'+\left(\mathrm{Ha}^2+S^2\right)\left(C-q^2\right)=0 \tag{18}$$

$$\left(1+\frac{K}{2}\right)g''+fg'-qg-K\left(2g+q'\right)=0 \tag{19}$$

$$\frac{1}{\mathrm{Pr}}\theta''+f\theta'+\mathrm{Ec}\left(1+\frac{1}{\beta}\right)q'^2+\mathrm{Ha}^2\mathrm{Ec}\left(C-q^2+B\theta\right)=0 \tag{20}$$

Subject to the boundary conditions (10) which become:

$$f(0)=0,\ \ q(0)=1,\ \ q(\infty)=C,\ \ \theta(0)=1,\ \ g(0)=-nq'(0),\ \ g(\infty)=0 \tag{21}$$

The system of non-linear differential eqs. (18) and (20) are solved under the boundary conditions which are given by eq. (21):

$$\left(1+\frac{k}{\mu}+\frac{1}{\beta}\right)\left[\frac{q_{i-1}-2q_i+q_{i+1}}{\Delta^2}\right]+\left(\mathrm{Ha}^2+S^2\right)\left(C-\overline{q_i}q_i\right)+$$
$$+\overline{f_i}\left[\frac{q_{i+1}-q_{i-1}}{2\Delta}\right]-\overline{q_i}q_i+K\left[\frac{g_{i+1}-g_{i-1}}{2\Delta}\right]=0 \tag{22}$$

$$\left(1+\frac{K}{2}\right)\left[\frac{g_{i-1}-2g_i+g_{i+1}}{\Delta^2}\right]+\overline{f_i}\left[\frac{g_{i+1}-g_{i-1}}{2\Delta}\right]-\overline{q_i}g_i-$$
$$-K\left(2g_i+\left[\frac{q_{i+1}-q_{i-1}}{2\Delta}\right]\right)=0 \tag{23}$$

$$\frac{1}{\mathrm{Pr}}\left[\frac{\theta_{i-1}-2\theta+\theta_{i+1}}{\Delta^2}\right]+f_i\left[\frac{\theta_{i+1}-\theta_{i-1}}{2\Delta}\right]+\mathrm{Ec}\left(1+\frac{1}{\beta}\right)\left[\frac{q_{i+1}-q_{i-1}}{2\Delta}\right]^2+$$
$$+\mathrm{Ha}^2E_c\left(C-\overline{q_i}q_i+B\theta_i\right)=0 \tag{24}$$

Results and discussion

This section is devoted to discuss the solutions by the aforementioned two methods, Firstly, the multi-step differential equation and secondly, FDM. After that a comparison between these two methods is computed, and offered in the following subsection.

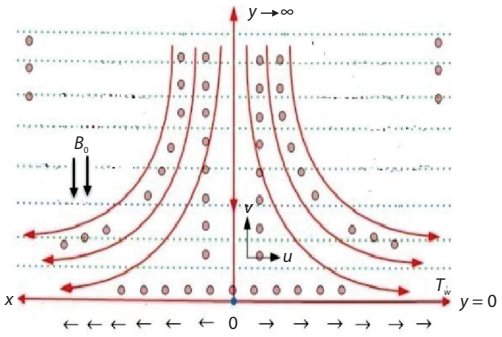

Figure 1. Physical flow diagram

Comparison between two numerical methods

The present investigation is used the FDM as well as the Ms-DTM methods. A detailed comparison between those methods was made to show agreement between them through figs. 1-3 and tab. 1. It is noticed from figs. 2-4. that the solutions of velocity, micro-rotation and temperature profiles evaluated

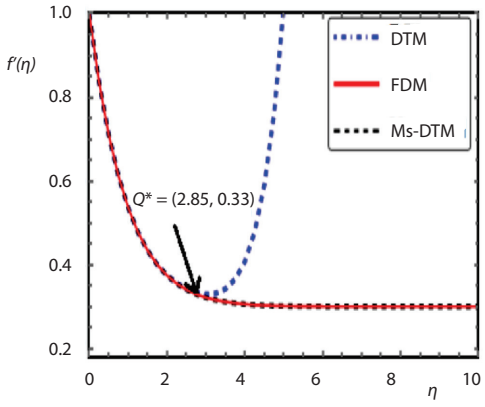

Figure 2. Behavior of velocity profile $f(\eta)$ against η for values $K = 0.1$, Ha = 0.3, Pr = 1, $B = 0.7$, $\beta = 0.3$, $S = 0.1$, Ec = 0.2, $n = 1$

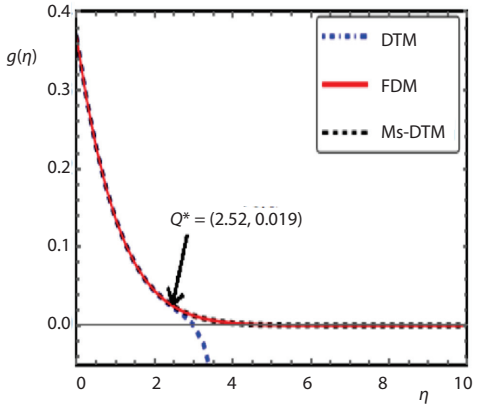

Figure 3. Behavior microrotation profile $g(\eta)$ against η for values $K = 0.1$, Ha = 0.3, Pr = 1, $B = 0.7$, $\beta = 0.3$, $S = 0.1$, Ec = 0.2, $n = 1$

by using DTM accept the behavior of numerical solution till a point Q, and then it diverges. So we utilize the Ms-DTM and FDM methods, those provide the solutions in terms of convergent series over a sequence of subintervals. In fact, our results indicate a close agreement between the FDM and Ms-DTM as shown in figs. 2-4 and tab. 1. Thereafter, the influences of physical parameters (the Casson parameter, β, the Hartmann number, Ha, the porous medium shape factor parameter, S, and the dimensionless heat generation/absorption parameter, B, on the velocity $f(\eta)$, microrotation, $g(\eta)$, and temperature profile, $\theta(\eta)$, by using Ms-DTM are illustrated through figs. 5-14. At what follows, the numerical estimations concern with the method of Ms-DTM, the target now is find the influences of various parameter for the previous distributions.

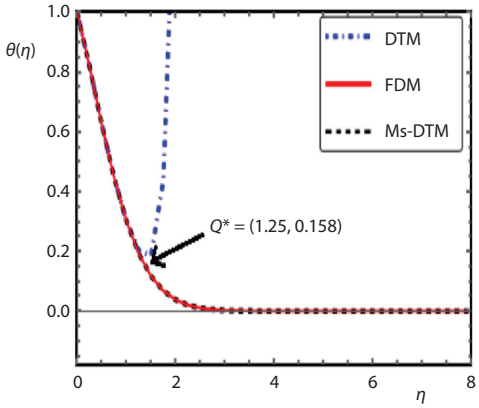

Figure 4. Behavior of temperature profile $\theta(\eta)$ against η for values $K = 0.1$, Ha = 0.3, Pr = 1, $B = 0.7$, $\beta = 0.3$, $S = 0.1$, Ec = 0.2, $n = 1$

For the velocity profile

Figures 5-7 are displayed to visualize the effect of various parameter on velocity profile. The calculation shows the following results:

- It is seen from figs. 5 and 6 that an increase in Casson parameter and Hartmann number causes on the velocity profile. Molecules of fluid cannot move easily without more energy.
- It is evident from the fig. 7 that an increase in porous medium shape factor parameter S causes an enhancement on the velocity profile.
- It is noted that the velocity profile have a slight difference for varying values of porous medium shape factor parameter S.
- It should be noted that the value of $S = 1$, the profile of the velocity distribution seems to be a straight line.

Table 1. Comparison between two numerical methods on a micropolar Casson fluid problem at $K = 0.1$, Ha = 0.3, Pr = 1, $B = 0.7$, $\beta = 0.3$, $S = 0.1$, Ec = 0.2, $n = 1$

η	$f'(\eta)$ FDM	$f'(\eta)$ Ms–Dtm	Error	$g(\eta)$ FDM	$g(\eta)$ Ms–Dtm	Error	$\theta(\eta)$ FDM	$\theta(\eta)$ Ms–Dtm	Error
0.	1.	1.	0.	0.367079	0.367091	0.0000123022	1.	1	0.
0.25	0.837335	0.837334	-4.94622×10^{-7}	0.28978	0.289788	8.23556×10^{-6}	0.819039	0.819043	4.11781×10^{-6}
0.5	0.710593	0.710592	-6.65241×10^{-7}	0.226899	0.226905	5.41505×10^{-6}	0.62455	0.624558	7.74406×10^{-6}
0.75	0.6123	0.612299	-6.59041×10^{-7}	0.176179	0.176183	3.49302×10^{-6}	0.446444	0.446454	0.0000100991
1.	0.536435	0.536435	-5.67497×10^{-7}	0.135642	0.135645	2.20787×10^{-6}	0.300934	0.300945	0.0000109063
1.25	0.478168	0.478168	-4.45107×10^{-7}	0.103554	0.103555	1.36594×10^{-6}	0.192244	0.192255	0.0000103407
1.5	0.433638	0.433637	-3.22307×10^{-7}	0.0783986	0.0783994	8.2637×10^{-7}	0.116874	0.116883	8.8528×10^{-6}
1.75	0.399775	0.399774	-2.14319×10^{-7}	0.0588694	0.0588699	4.88704×10^{-7}	0.0678501	0.067857	6.9568×10^{-6}
2.	0.374151	0.374151	-1.27113×10^{-7}	0.0438522	0.0438525	2.82734×10^{-7}	0.0377198	0.0377249	5.07266×10^{-6}
2.25	0.354857	0.354857	-6.13522×10^{-8}	0.0324121	0.0324122	1.60454×10^{-7}	0.0201275	0.0201309	3.4581×10^{-5}
2.5	0.3404	0.3404	-1.49425×10^{-8}	0.0237758	0.0237759	8.98017×10^{-8}	0.0103294	0.0103316	2.21569×10^{-6}
2.75	0.329621	0.329621	1.53931×10^{-8}	0.0173132	0.0173133	4.99025×10^{-8}	0.00510738	0.00510872	1.33877×10^{-6}
3.	0.321621	0.321621	3.31827×10^{-8}	0.0125183	0.0125183	2.75483×10^{-8}	0.00243723	0.00243799	7.63733×10^{-7}
3.25	0.315712	0.315712	4.17019×10^{-8}	0.00898955	0.00898957	1.46496×10^{-8}	0.00112442	0.00112483	4.10413×10^{-7}
3.5	0.311368	0.311368	4.37404×10^{-8}	0.00641309	0.00641309	6.43692×10^{-9}	0.000502499	0.000502705	2.05802×10^{-7}
3.75	0.308189	0.308189	4.15324×10^{-8}	0.00454608	0.00454608	2.24776×10^{-10}	0.000218034	0.000218128	9.36455×10^{-8}
4.	0.305873	0.305873	3.6778×10^{-8}	0.00320295	0.00320295	-5.41458×10^{-9}	0.0000921164	0.0000921517	3.5282×10^{-8}
4.25	0.304194	0.304194	3.07117×10^{-8}	0.00224341	0.0022434	-1.11866×10^{-8}	0.0000380308	0.0000380372	6.39963×10^{-9}
4.5	0.302982	0.302982	2.41869×10^{-8}	0.00156245	0.00156244	-1.74088×10^{-8}	0.0000154129	0.0000154057	-7.19174×10^{-9}
4.75	0.302111	0.302111	1.77615×10^{-8}	0.00108228	0.00108225	-2.42113×10^{-8}	6.16575×10^{-6}	6.1525×10^{-6}	-1.32503×10^{-8}
5.	0.301488	0.301488	1.17737×10^{-8}	0.000745743	0.000745711	-3.16494×10^{-8}	2.45041×10^{-6}	2.43464×10^{-6}	-1.57746×10^{-8}
5.25	0.301044	0.301044	6.40675×10^{-9}	0.000511254	0.000511214	-3.97634×10^{-8}	9.74224×10^{-7}	9.57507×10^{-7}	-1.67169×10^{-8}
5.5	0.30073	0.30073	1.73957×10^{-9}	0.00034878	0.000348732	-4.86052×10^{-8}	3.90058×10^{-7}	3.73075×10^{-7}	-1.6983×10^{-8}
5.75	0.300507	0.300507	-2.21407×10^{-9}	0.000236809	0.000236751	-5.82483×10^{-8}	1.5811×10^{-7}	1.41135×10^{-7}	-1.69742×10^{-8}
6.	0.300351	0.300351	-5.47732×10^{-9}	0.00016004	0.000159972	-6.87883×10^{-8}	6.50826×10^{-8}	4.82223×10^{-8}	-1.68603×10^{-8}
6.25	0.300242	0.300242	-8.09021×10^{-9}	0.000107668	0.000107588	-8.03399×10^{-8}	2.72147×10^{-8}	1.05044×10^{-8}	-1.67103×10^{-8}
6.5	0.300166	0.300166	-1.00963×10^{-8}	0.0000721112	0.0000720182	-9.30328×10^{-8}	1.15374×10^{-8}	-5.01347×10^{-9}	-1.65508×10^{-8}
6.75	0.300113	0.300113	-1.1534×10^{-8}	0.000048083	0.0000479759	-1.07008×10^{-7}	4.94152×10^{-9}	-1.14505×10^{-8}	-1.6392×10^{-8}
7.	0.300077	0.300077	-1.24318×10^{-8}	0.0000319188	0.0000317964	-1.22416×10^{-7}	2.12976×10^{-9}	-1.41075×10^{-8}	-1.62373×10^{-8}
7.25	0.300052	0.300052	-1.28054×10^{-8}	0.0000210928	0.0000209534	-1.39414×10^{-7}	9.20213×10^{-10}	-1.51674×10^{-8}	-1.60876×10^{-8}
7.5	0.300035	0.300035	-1.26564×10^{-8}	0.000013873	0.0000137149	-1.58165×10^{-7}	3.97364×10^{-10}	-1.55458×10^{-8}	-1.59431×10^{-8}
7.75	0.300023	0.300023	-1.19726×10^{-8}	9.07789×10^{-6}	8.89905×10^{-6}	-1.78839×10^{-7}	1.71081×10^{-10}	-1.56326×10^{-8}	-1.58037×10^{-8}
8.	0.300016	0.300015	-1.07283×10^{-8}	5.90549×10^{-6}	5.70388×10^{-6}	-2.01612×10^{-7}	7.33117×10^{-11}	-1.55958×10^{-8}	-1.56691×10^{-8}
8.25	0.30001	0.30001	-8.88447×10^{-9}	3.81402×10^{-6}	3.58735×10^{-6}	-2.26667×10^{-7}	3.12271×10^{-11}	-1.55078×10^{-8}	-1.5539×10^{-8}
8.5	0.300007	0.300007	-6.39011×10^{-9}	2.43915×10^{-6}	2.18496×10^{-6}	-2.54193×10^{-7}	1.32041×10^{-11}	-1.54×10^{-8}	-1.54132×10^{-8}
8.75	0.300004	0.300004	-3.18245×10^{-9}	1.53698×10^{-6}	1.2526×10^{-6}	-2.84389×10^{-7}	5.53081×10^{-12}	-1.5286×10^{-8}	-1.52915×10^{-8}
9.	0.300003	0.300003	8.12329×10^{-10}	9.4496×10^{-7}	6.27499×10^{-7}	-3.17461×10^{-7}	2.28357×10^{-12}	-1.51713×10^{-8}	-1.51735×10^{-8}
9.25	0.300002	0.300002	5.67871×10^{-9}	5.55196×10^{-7}	2.0157×10^{-7}	-3.53626×10^{-7}	9.16829×10^{-13}	-1.50583×10^{-8}	-1.50592×10^{-8}
9.5	0.300001	0.300001	1.15115×10^{-8}	2.96387×10^{-7}	-9.67227×10^{-8}	-3.9311×10^{-7}	3.43543×10^{-13}	-1.4948×10^{-8}	-1.49483×10^{-8}
9.75	0.3	0.3	1.84159×10^{-8}	1.21589×10^{-7}	-3.14561×10^{-7}	-4.36149×10^{-7}	1.02666×10^{-13}	-1.48405×10^{-8}	-1.48406×10^{-8}
10.	0.3	0.3	2.65071×10^{-8}	0.	-4.82992×10^{-7}	-4.82992×10^{-7}	0.	-1.4736×10^{-8}	-1.4736×10^{-8}

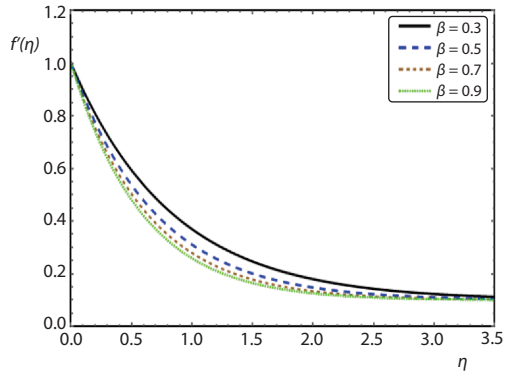

Figure 5. Behavior of velocity profile $f(\eta)$ against η for several values $K = 0.1$, Ha = 0.3, Pr = 1, $B = 0.7$, $S = 0.1$, Ec = 0.2, $n = 1$

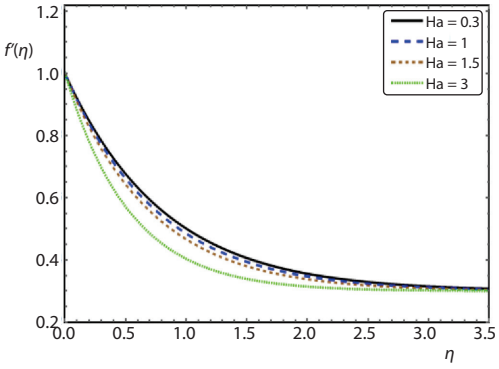

Figure 6. Behavior of velocity profile $f(\eta)$ against η for several values $K = 0.1$, Pr = 1, $\beta = 0.7$, $S = 0.1$, Ec = 0.2, $n = 1$

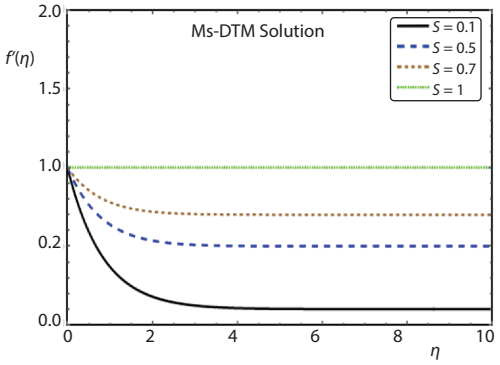

Figure 7. Behavior of velocity profile $f(\eta)$ against η for several values $K = 0.1$, Ha = 0.3, Pr = 1, $B = 0.7$, $\beta = 0.2$, Ec = 0.2, $n = 1$

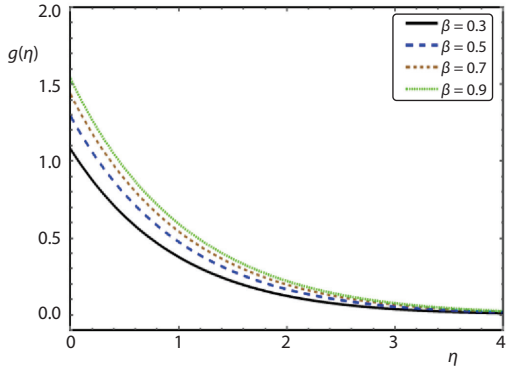

Figure 8. Behavior of microrotation profile $g(\eta)$ against η for several values $K = 0.1$, Ha = 0.3, Pr = 1, $B = 0.7$, $S = 0.2$, Ec = 0.2, $n = 1$

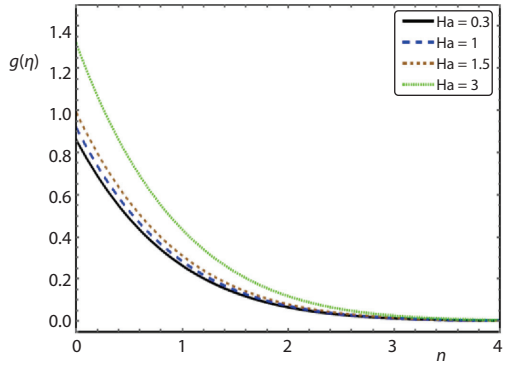

Figure 9. Behavior of microrotation profile $g(\eta)$ against η for several values $K = 0.1$, Pr = 1, $B = 0.7$, $\beta = 0.2$, $S = 0.2$, Ec = 0.2, $n = 1$

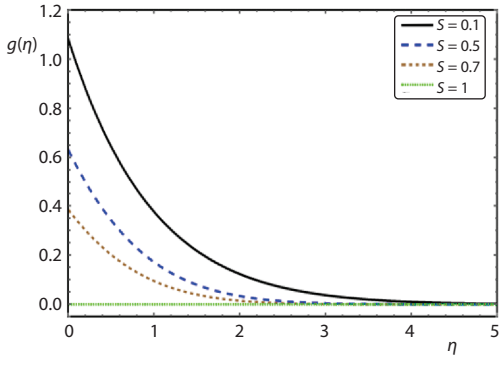

Figure 10. Behavior of microrotation profile $g(\eta)$ against η for several values $K = 0.1$, Ha = 0.3, Pr = 1, $B = 0.7$, $\beta = 0.2$, Ec = 0.2, $n = 1$

For the microrotation profile graphed

Figures 8-10 are displayed to visualize the effect of various parameter on microrotation profile. the numerical calculations draw the following results:

– The impact of β and Ha are portrayed in figs. 8 and 9. It is show that the higher values of β and enhances the microrotation profile.
– The increasing of S on microrotation profile $g(\eta)$ increases as in fig. 10.

For the temperature profile graphed

Figures 11-14 disclosed the impact of β, Ha, S, and B on the temperature profile:

– The behavior of β and Ha on the temperature $\theta(\eta)$ are depicted in figs. 11 and 12. Here the effect of increasing β and Ha that leads to an increase in temperature profile.
– The fluid temperature at increases with the increase of the heat generation parameter B, as shown in fig. 13.
– Larger S reduces $\theta(\eta)$ which results in argumentation of heat transfer at the wall as shown in fig. 14.
– It is noted that the temperature profile has a sight difference for various values of S.

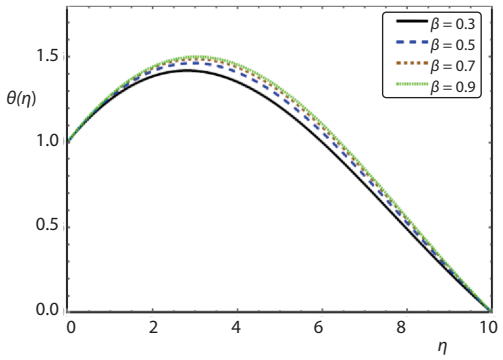

Figure 11. Behavior of temperature profile $\theta(\eta)$ against η for several values $K = 0.1$, Ha = 0.3, Pr = 1, $B = 0.7$, $S = 0.2$, Ec = 0.2, $n = 1$

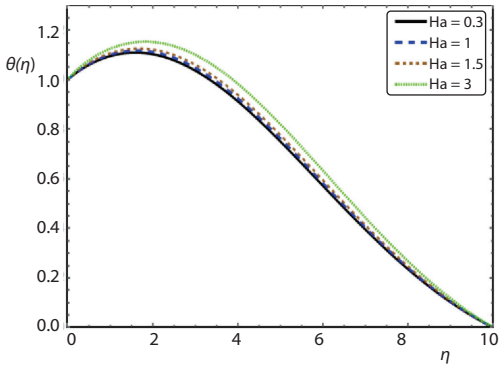

Figure 12. Behavior of temperature profile $\theta(\eta)$ against η for several values $K = 0.1$, Pr = 1, $B = 0.7$, $\beta = 0.2$, $S = 0.2$, Ec = 0.2, $n = 1$

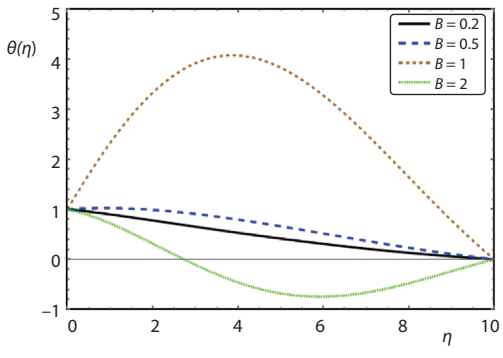

Figure 13. Behavior of temperature profile $\theta(\eta)$ against η for several values $K = 0.1$, Ha = 0.3, Pr = 1, $\beta = 0.2$, $S = 0.1$, Ec = 0.2, $n = 1$

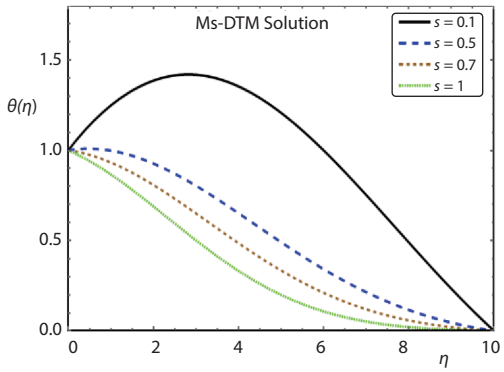

Figure 14. Behavior of temperature profile $\theta(\eta)$ against η for several values $K = 0.1$, Ha = 0.3, Pr = 1, $B = 0.7$, $\beta = 0.2$, Ec = 0.2, $n = 1$

Conclusions

The current paper investigates an incompressible micropolar Casson fluid over a stretching surface. Porous medium and heat generation are taken into consideration. The governing equations of motion are analytically solved through Ms-DTM to obtain the distribution of velocity, microrotation and temperature. The Ms-DTM are applicable to non-linear models such as micropolar Casson fluid models which is more complicated and have a higher degree of non-linearity, in a direct way without using linearization or restrictive assumptions. The velocity, microrotation in space-time domain and temperature are obtained for different times and for various values of material parameters using a Ms-DTM. The investigation draws the following concluding remarks.

- The influences of β and Ha on $f'(\eta)$ are similar in a qualitative sense.
- Temperature and microrotation are reduced for higher values of S.
- At $S = 1$, it is seen that no variation for the velocity and microrotation parameter profiles. Therefore, they graphed a horizontal straight line.
- The advantage of the Ms-DTM is to make a linearization for the non-linear system. Therefore, away from any other methods, we can easily solve the problem.
- An accuracy comparison is made between the methods of FDM and Ms-DTM. This comparison shows that the error between them is efficiently small.

Nomenclature

B – dimensionless heat generation/absorption parameter
B_0 – a uniform magnetic field
c_p – specific heat at constant pressure
Da – Darcy number
Ec – Eckert number
Ha – Hartmann number
K – dimensionless velocity ratio parameter
K_d – Darcy permeability
k – thermal diffusivity
Pr – Prandtl number
S – porous medium shape factor parameter
N – microrotation vector
n – boundary concentration parameter of fluid
T_∞ – temperature at infinity
T_w – temperature at the stretched plane

Greek symbols

γ – electric conductivity
μ – spin gradient viscosity
ρ – fluid density

References

[1] Eringen, A. C., Theory of Micropolar Fluids, *Journal of Mathematical Mechanics*, *16* (1966), 1, pp. 1-18
[2] Ali, N., Hayat, T., Peristaltic Flow of a Micropolar Fluid in an Asymmetric Channel, *Computer and Applied Math*., *55* (2008), 4, pp. 589-608
[3] Ahmad, S., *et al*., Effects of Thermal Radiation on MHD Axisymmetric Stagnation Point Flow and Heat Transfer of a Micropolar Fluid over a Shrinking Sheet, *World Applied Sciences Journal*, *15* (2011), 6, pp. 835-848
[4] Eldabe, N. T., Abou-Zeid, M. Y., Magnetohydrodynamic Peristaltic Flow with Heat and Mass Transfer of Micropolar Biviscosity Fluid through a Porous Medium between Two Co-Axial Tubes, *Arab Journal Science Engineering*, *39* (2014), Apr., pp. 5045-5062
[5] Nazeer, M., *et al*., Numerical Simulation of MHD Flow of Micropolar Fluid Inside a Porous Inclined Cavity with Uniform and Non-Uniform Heated Bottom Wall, *Can J. Phys*., *96* (2017), 6, pp. 576-593
[6] Mishra, S. R., *et al*., Free Convective Micropolar Fluid-Flow and Teat Transfer over a Shrinking Sheet with Heat Source, *Case Studies in Thermal Engineering*, *11* (2018), Mar., pp. 113-119
[7] Ali, N., *et al*., Buoyancy Driven Cavity Flow of a Micropolar Fluid with Variably Heated Bottom Wall, *Heat Trans. Res*., *49* (2018), 5, pp. 457-481
[8] Nazeer, M., Numerical Simulations of MHD Forced Convection Flow of Micropolar Fluid Inside a Right Angle Triangular Cavity Saturated with Porous Medium: Effects of Vertical Moving Wall, *Can. J. Phys*., *97* (2018), 1, pp. 1-25

[9] Khan, N. A., *et al*., Flow of Micropolar Fluid over an off Centred Rotating Disk with Modified Darcy's Law, *Propulsion and Power Research*, *6* (2017), 4, pp. 285-295
[10] Khan, N. A., *et al*., Entropy Generation Analysis and of Slip Conditions on Micropolar Fluid-Flow Due to a Rotating Disk, *Open Engineering*, *7* (2017), 1, pp. 185-198
[11] Asad, M., *et al*., Hydromagnetic Hiemenz Flow of Micropolar Fluid over a Non-Linearly Stretching/Shrinking Sheet: Dual Solutions by Using Chebyshev Spectral Newton Iterative Scheme, *Journal of Magnetism and Magnetic Materials*, *416* (2016), Oct., pp. 329-334
[12] Shah, Z., *et al*., The Electrical MHD and Hall Current Impact on Micropolar Fanofluid-flow between Rotating Parallel Plates, *Results in Physics, 9* (2018), June, pp. 1201-1214
[13] El-Dabe, N. T. M., *et al*., Heat and Mass Transfer of Magnetohydrodynamic Pulsatile Flow of Casson Fluid with Couple Stress through Porous Medium, *International Journal of Current Engineering and Technology*, *6* (2016), 4, pp. 1414-1421
[14] Mekheimer, K. S., Non-Linear Peristaltic Transport through a Porous Medium in an Inclined Planar Channel, *Journal of Porous Media*, *6* (2003), 3, pp. 190-202
[15] Zueco, J., Ahmed, S., Combined Heat and Mass Transfer by Mixed Convection MHD Flow Along a Porous Plate with Chemical Reaction in Presence of Heat Source, *Applied Mathematics and Mechanics, 31* (2010), Oct., pp. 1217-1230
[16] El-Dabe, N. T. M., *et al*., Effect of Partial Slip on Peristaltic Flow of a Sisko Fluid with Mild Stenosis through a Porous Medium, *Applied Mathematics and Information Sciences*, *10* (2016), 2, pp. 673-687
[17] Vinogradov, G. V., Malkin, A. Y., *Rheology of Polymers*, Mir Publisher, Moscow, Russia, 1979
[18] Mehmoo, Z., *et al*., Numerical Investigation of Micropolar Casson Fluid over a Stretching Sheet with Internal Heating, *Communication Theory of Physics*, *67* (2017), 4, pp. 443-448
[19] Iqbal, Z., *et al*., Impact of Inclined Magnetic Field on Micropolar Casson Fluid Using Keller Box Algorithm, *The European Physical Journal Plus*, *15* (2017), Apr., pp. 132-175
[20] Hiemenz, K., Die Grenzschict neinem in den gleichformigen flussigkeitsstrom eingetauchten geraden Kreiszylinder (in German), *Dingler's Polytech Journal*, *326* (1911), pp. 321-410
[21] Shateyi, S., Makinde, O. D., Hydromagnetic Stagnation-Point Flow Towards a Radially Ctretching Convectively Heated Disk, *Mathematical Problems in Engineering*, *2013* (2013), ID616947
[22] Bhattacharyy, K., *et al*., Slip Effects on Boundary-Layer Stagnation-Point Flow and Heat Transfer Towards a Shrinking Sheet, *International Journal physics of Heat and Mass Transfer*, *54* (2011), 1-3, pp. 308-313
[23] Motsa, S. S., Shateyi, K. Y. S., A New Numerical Solution of Maxwell Fluid over a Shrinking Sheet in the Region of a Stagnation Point, *Mathematical Problems in Engineering*, *2012* (2012), ID290615
[24] Javed, T., Ghaffari, A., Numerical Study of Non-Newtonian Maxwell Fluid in the Region of Oblique Stagnation Point Flow over a Stretching Sheet, *Journal of Mechanics*, *32* (2016), 2, pp. 175-184
[25] Mustafa, I., *et al*., Heat Transfer in MHD Stagnation Point Flow of a Ferrofluid over a Stretchable Rotating Disk, *Journal of Molecular Liquids*, *219* (2016), July, pp. 526-532
[26] Ghaffari, A., *et al*., Heat Transfer Analysis of Unsteady Oblique Stagnation Point Flow of Elastico-Viscous Fluid Due to Sinusoidal Wall Temperature over an Oscillating-Stretching Surface: A Numerical Approach, *Journal of Molecular Liquids*, *219* (2016), July, pp. 748-755
[27] Tasaka, Y., *et al*., Experimental Investigation of Natural-Convection Induced by Internal Heat Generation, *Proceedings,* 14th, Inter. Couete Taylor Workshop, Sapporo, Japan, 2005, Vol. 14, pp. 168-79
[28] Crepeau, J. C., Clarksean, R., Similarity Solutions of Natural-Convection with Internal Heat Generation, Trans ASME, *Journal of Heat Transfer*, *119* (1997), 1, pp. 184-185
[29] Salem, A. M., El-Aziz, M. A., The MHD-Mixed Convection and Mass Transfer from a Vertical Stretching Sheet with Diffusion of Chemically Reactive Species and Space or Temperature Dependent Heat Source, *Canadian Journal of Physics*, *85* (2007), 4, pp. 359-373
[30] Salem, A. M., El-Aziz, M. A., Effect of Hall Currents and Chemical Reaction on Hydromagnetic-Flow of a Stretching Vertical Surface with Internal Heat Generation/Absorption, *Applied Mathematical Modelling*, *32* (2008), 7, pp. 1236-1254
[31] Muhammad, S., *et al*., The Rotating Flow of Magneto Hydrodynamic Carbon Nanotubes over a Stretching Sheet with the Impact of Non-Linear Thermal Radiation and Heat Generation/Absorption, *Applied Sciences*, *8* (2018), 4, 82
[32] Ghaffari, A., Enhancement of Heat Transfer in Elastico-Viscous Fluid Due to Nanoparticles, where the Fluid is Impinging Obliquely to the Stretchable Surface: A Numerical Study, *Applications and Applied Mathematics*, *11* (2016), 1, pp. 251-265

[33] Shah, Z., *et al*., The 3-D Third Grade Nanofluid-Flow in a Rotating System between Parallel Plates with Brownian Motion and Thermophoresis Effects, *Results in Physics*, *10* (2018), Sept., pp. 36-45
[34] Shah, Z., Islam, S., Effects of Hall Current on Steady 3-D Non-Newtonian Nanofluid in a Rotating Frame with Brownian Motion and Thermophoresis Effects, *Journal of Engineering Technology*, *6* (2017), pp. July, 280-296
[35] Ali, N., *et al*., Flow and Heat Transfer Analysis of Eyring-Powell Fluid in a Pipe, *Zeitschrift für Naturforschung A (ZNA)*, *73* (2018), 3, pp. 265-274
[36] Ishaq, M., *et al*., Entropy Generation on Nanofluid Thin Film Flow of Eyring-Powell Fluid with Thermal Radiation and MHD Effect on an Unsteady Porous Stretching Sheet, *Entropy*, *20* (2018), 6, pp. 412-436
[37] Nasir, S., *et al*., The 3-D Rotating fow of MHD Single Wall Carbon Nanotubes over a Stretching Sheet in Presence of Thermal Radiation, *Applied Nanoscience*, *8* (2018), May, pp. 1361-1378
[38] Odibat, Z. M., *et al*., A Multistep Differential Transform Method and Application Non-Chaotic or Chaotic Systems, *Computers and Mathematics with Applications*, *59* (2010), 4, pp. 1462-1472
[39] Zait, R. A., *et al*., Statistical Measures Approximations for the Gaussian Part of the Stochastic Non-Linear Damped Duffing Oscillator Solution Process under the Application of Wiener Hermite Expansion Linked by the Multi-Step Differential Transformed Method, *Journal of the Egyptian Mathematical Society*, *24* (2016), 3, pp. 1-12
[40] Courant, R., *et al*., Uber die partiellen differenzengleichungen der mathematischen physik (in German), *Mathematische Annalen*, *100* (1928), pp. 32-74
[41] Le Veque, R. J., *Finite Difference Methods for Ordinary and Partial Differential Equations*, Society for Industrial and Applied Mathematics, Washington, USA, 2007
[42] Thomee, V., From Finite Differences to Finite Elements a Short History of Numerical Analysis of Partial Differential Equations, *Journal of Computational and Applied Mathematics, 128* (2001), 1-2, pp. 1-54

Paper submitted: January 13, 2018
Paper revised: October 13, 2018
Paper accepted: December 15, 2018